Large-Stroke Dielectric Elastomer Actuators With Ion-Implanted Electrodes

Samuel Rosset, Muhamed Niklaus, Philippe Dubois, and Herbert R. Shea, *Senior Member, IEEE*

***Abstract*—In this paper, we present miniaturized polydimethylsiloxane (PDMS)-based diaphragm dielectric elastomer actuators capable of out-of-plane displacement up to 25% of their diameter. This very large percentage displacement is made possible by the use of compliant electrodes fabricated by low-energy gold ion implantation. This technique forms nanometer-scale metallic clusters up to 50 nm below the PDMS surface, creating an electrode that can sustain up to 175% strain while remaining conductive yet having only a minimal impact on the elastomer's mechanical properties. We present a vastly improved chip-scale process flow for fabricating suspended-membrane actuators with low-resistance contacts to implanted electrodes on both sides of the membrane. This process leads to a factor of two increase in breakdown voltage and to RC time constant shorter than mechanical time constants. For circular diaphragm actuator of 1.5–3-mm diameter, voltage-controlled static out-of-plane deflections of up to 25% of their diameter is observed, which is a factor of four higher than our previous published results. Dynamic characterization shows a mechanically limited behavior, with a resonance frequency near 1 kHz and a quality factor of 7.5 in air. Lifetime tests have shown no degradation after more than 4 million cycles at 1.5 kV. Conductive stretchable electrodes photolithographically defined on PDMS were demonstrated as a key step to further miniaturization, enabling large arrays of independent diaphragm actuators on a chip, for instance for tunable microlens arrays or arrays of micropumps and microvalves. [2009-0107]**

***Index Terms*—Dielectric elastomer actuators (DEAs), electroactive polymers (EAPs), filtered cathodic vacuum arc (FCVA), metal ion implantation.**

I. Introduction

DIELECTRIC elastomer actuators (DEAs) are a class of electroactive-polymer (EAP) actuators (also known as artificial muscles) that posses particularly appealing properties, combining large displacements (up to several hundred percent strain) and high actuation pressure per unit mass (about 10^3 Pa $\cdot$ m^3/kg) with low energy consumption [1], [2]. DEAs consists of a soft elastomer sandwiched between two compliant electrodes. Applying a voltage between the two electrodes generates a compressive electrostatic stress, which squeezes the elastomeric dielectric, thus causing a thickness decrease and a surface expansion in the case of free-boundary conditions (Fig. 1).

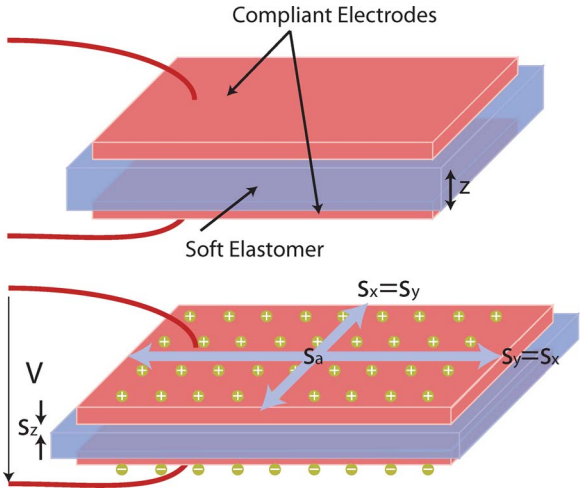

Fig. 1. Dielectric-EAP principle. When a voltage is applied to the electrodes (typically up to 1 kV), the electrostatic pressure squeezes the elastomer dielectric (negative thickness strain, s_z) (right side). The volume of the dielectric being constant, the whole structure stretches in the case of free-boundary conditions (positive area strain s_a, as well as in-plain strains s_x and s_y).

Because of their intrinsic linear actuation, low mass, as well as energy density comparable to that of natural muscles, DEAs can be used in numerous applications, such as artificial muscles for humanlike robots [3] or for rehabilitation purposes [4]. DEAs are possible substitutes for electromagnetic motors in applications which require linear motion, such as robot manipulators [5], [6] or samples manipulators for magnetic resonance imaging [7], whose strong electromagnetic fields make use of conventional motors impossible. Most of the DEAs presented in the literature are macroscale devices, with sizes ranging from square meters (e.g., in a large blimp project of the Swiss Federal Laboratories for Materials Testing and Research [8]) to square centimeters for small positioners.

While there are many examples of macroscale DEAs, the literature on miniaturized DEAs is sparse, mainly due to the lack of an appropriate technology to make microelectromechanical-systems (MEMS)-compatible compliant electrodes. However, the miniaturization of DEAs is very promising, as these actuators would combine characteristics unmatched by any other mainstream MEMS actuator types, particularly large displacement, elasticity, and high energy density.

The important requirements that compliant electrodes for DEAs must meet are as follows: 1) a high conductivity which is maintained when the electrode is deformed; 2) a low impact on the mechanical properties of the elastomer; and 3) a small thickness relative to that of the polymer [9]. The general compromise

Manuscript received April 26, 2009; revised August 14, 2009. First published October 16, 2009; current version published December 1, 2009. This work was supported in part by the Swiss National Science Foundation under Grant 200020-120164 and in part by the Ecole Polytechnique Fédérale de Lausanne (EPFL). Subject Editor R. T. Howe.

The authors are with the Microsystems for Space Technologies Laboratory, Ecole Polytechnique Fédérale de Lausanne, 1015 Lausanne, Switzerland (e-mail: samuel.rosset@a3.epfl.ch; muhamed.niklaus@epfl.ch; philippe.dubois@unine.ch; herbert.shea@epfl.ch).

Color versions of one or more of the figures in this paper are available online at http://ieeexplore.ieee.org.

Digital Object Identifier 10.1109/JMEMS.2009.2031690

for macroscale applications is to use electrodes based on carbon powders (either carbon black applied with a stamp or spray or carbon powder mixed with grease or unpolymerized elastomer [10]–[12]). However, this technology is not suited to miniaturize DEAs which requires electrodes that can be patterned on a millimeter to micrometer scale. Although small-scale patterning has been successfully performed with carbon black by pattern transfer on a polydimethylsiloxane (PDMS) stamp [12] or by spraying of graphite powder through a shadow mask [13], [14], the mechanical adhesion of the powder on the elastomer is problematic in the case of silicon elastomers [11] (as opposed to the widely used sticky VHB tape), without mentioning the difficulty to work cleanly with carbon powders, which is essential to avoid short-circuits between electrodes, particularly when the size of the device is reduced.

Standard metal thin-film deposition, such as e-beam evaporation or cathodic sputtering, which leads to highly conductive layers easily patternable by photolithography or with a shadow mask, is not applicable to DEAs. Plain metallic thin films do not fulfill one of the crucial requirements of DEAs' electrodes: The ability to sustain large deformations without damage. Indeed, the maximal strain that a metal thin-film track can sustain before breaking is typically limited around 2%–3%. To overcome this limitation, some research groups have patterned their thin-film electrodes in z-shape [15] or in concentric rings [16] over the actuator's surface. By using their optimized electrodes patterned in concentric rings, Pimpin *et al.* [16] obtained a maximal displacement which was 11.2 times higher than when using a plain thin-film electrode. However, even when patterned, the metal thin film has an important impact on the Young's modulus of the structure, due to the four to five order of magnitude between the Young's modulus of metal and that of the elastomer typically used to make DEAs. This leads to reduced strains compared to an actuator with carbon-based electrodes.

We have introduced low-energy metal ion implantation on PDMS as a method which combines compatibility with a microfabrication processes, ease of patterning, and high electrical conductivity with a low impact on the mechanical properties of the elastomer and a high maximal strain before loss of conductivity. The implantation leads to the creation of nanometer-size clusters which extends from the surface of the PDMS down to approximately 50 nm [17]. Similar to the case of carbon powder, the metallic clusters are physically in contact (thus creating electrical conduction paths), without being mechanically bound to each other, thus limiting the stiffening impact of the implantation on the PDMS. When the implanted layer is strained, the clusters can easily move relative to each other while keeping a conduction path. We tested three different metals: titanium, gold, and palladium. Gold-implanted layers were shown to combine the best overall characteristics, with a low time-stable sheet resistance (0.1–1 $\mathrm{k}\Omega/\mathrm{square}$), large maximal strain before loss of conductivity (175%), and a limited impact on the Young's modulus of the PDMS (50%–100% relative increase) [18].

We have demonstrated [19] and characterized [20] the use of ion-implanted electrodes for miniaturized DEAs through buckling diaphragm actuators capable of out-of-plane deflection. In this paper, we report on a completely redesigned process flow which—in combination with the implantation's optimization—enabled us to obtain out-of-plane deflections up to 25% of our circular actuators' diameter ($\varnothing$1.5–3 mm). The new actuator generation also presents much higher dynamic-response speeds of around 1 ms, whereas our previous devices were characterized by inconsistent response speeds between 15 and 500 ms.

II. Ion Implantation

As elastomers used for DEAs have a low density (0.9–1.2 $\mathrm{g/cm^3}$), heavy metallic ions can easily penetrate the polymer matrix. Consequently, low ion energies must be used to keep the ions close to the surface, as required to create electrodes for DEAs. An energy below 8 keV is desirable in order to confine the ions in the first tens of nanometers below the PDMS surface. For our gold-implanted electrodes, we have used a beam with a broad energy distribution between 50 eV and 5 keV. This allows the obtaining of a continuous distribution of ions between the PDMS surface and a depth of about 50 nm.

In addition to low ion energy, the implantation must be conducted with a high ion flux in order to reach the desired dose for good conductivity $(1 \cdot 10^{16}$–$5 \cdot 10^{16}$ $\mathrm{at/cm^2})$ in a reasonable amount of time. Unfortunately, typical classical (ion beam) implantation machines have a very low ion flux at low energies and can generally not produce a stable beam below 10 keV. When implanting metal ions into soft elastomers at energies of 10 keV or above, the ions cannot be confined close to the surface, and the implantation time can become very long in order to reach a volumic density of metallic particles high enough to create a conductive layer. This leads to implantations lasting from a couple of hours to several days, which makes these implanters practically and economically unsuitable for our application.

Consequently, a plasma-based technique of implantation named filtered cathodic vacuum arc (FCVA) and based on a pulsed-vacuum-arc plasma source was selected to make the implantations. This implantation technology was pioneered by Aksenov *et al.* [21] and studied in details by Brown *et al.* [22]–[26] at the Lawrence Berkeley Laboratory. An FCVA system consists of a plasma gun, a magnetic filter, and electronics to generate the electrical signals. Operation of the plasma gun takes place in high vacuum $(\sim 10^{-6}$ mbar). In our pulsed system (Fig. 2), a charged capacitor tank applies 600 V between the anode and the cathode (source of the material to be deposited). The applied electrical field between the two electrodes is smaller than the breakdown field in vacuum. Hence, no current flows between the two electrodes. The arc is initiated by a high-voltage (HV) pulse (10–18 kV) on the trigger electrode, which is situated in close proximity of the cathode. This small plasma initiates the main arc between the cathode and the anode, which discharges the tank capacitor in 600 μs with a current of 50–100 A, leading to the production of a dense plasma of the cathode material. The drifting plasma enters an electromagnetic filter, which consists of a 90°-bent flexible vacuum bellow, around which a 15-turns coil is wound. The coil is connected in series with the anode terminal, thus automatically producing a steering magnetic field during the arc duration. The magnetic field guides the electrons and ions through the duct, but the large macroparticles which are unavoidably produced during the arc are not affected by the field, due to their large mass-over-charge

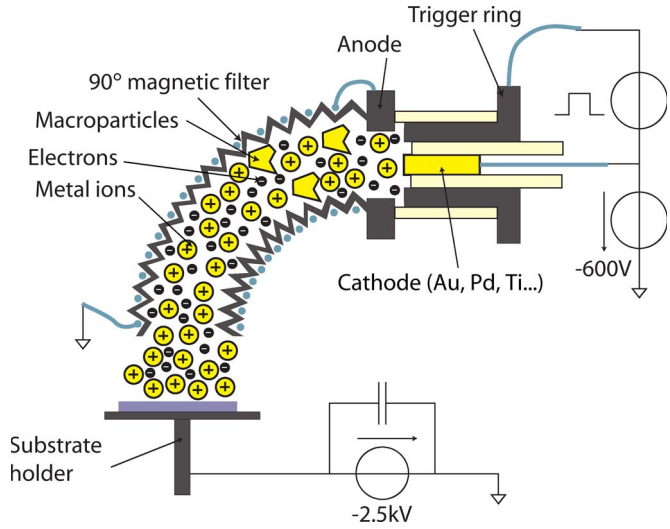

Fig. 2. Schematic representation of our FCVA implanter. An HV pulse on the trigger electrode initiates the main arc between the source (cathode) and the anode. The electrons, ions, and macroparticles produced by the arc enter the filter which traps the macroparticles. The substrate holder is negatively biased to accelerate the positive ions through the plasma sheath.

ratio [22], [23], [26]. They consequently collide with the filter's walls and do not reach the surface, which ensures a pure ion implantation.

Selective implantation of the PDMS surface can be achieved by the use of a shadow mask or with photoresist (PR) mask defined by photolithography for better resolutions. Gold was used for all the implantations presented in this paper, with broad ion energy distribution, ranging between 50 eV and 5 keV. This leads to an almost-constant volumic concentration in the first 50 nm of the PDMS layer [17]. The implantation time is around 5 min for a sheet resistance between 200 and 1000 Ω/square, with a relative increase of the PDMS Young's modulus below 100% for 30-μm-thick layer of PDMS with an initial Young's modulus around 1 MPa. To obtain high implantation homogeneity, despite the Gaussian ion-beam profile and small diameter (1–1.5 cm), a motorized scanning stage is used in the vacuum chamber to move the sample under the beam during the implantation.

III. Actuator Design and Fabrication

A. Concept and Model

Using the implantation technique, buckling-mode actuators with ion-implanted electrodes were fabricated. They consist of a DEA structure (electrode–dielectric–electrode, see Fig. 1) bonded on a Pyrex chip with circular through-holes of diameter $\varnothing$1.5–3 mm. The initially flat membrane buckles when a voltage is applied to the electrodes, because the clamped boundary condition prevents the in-plane area expansion (Fig. 3, top). The amplitude of the membrane's out-of-plane deflection depends on the applied voltage, as well as the membrane's mechanical and geometrical parameters. If a distributed force is applied on one side of the membrane (for example, by applying a pressure difference between the two sides of the membrane), the membrane will deform into a spherical dome whose amplitude depends on the applied voltage and pressure (Fig. 3, bottom).

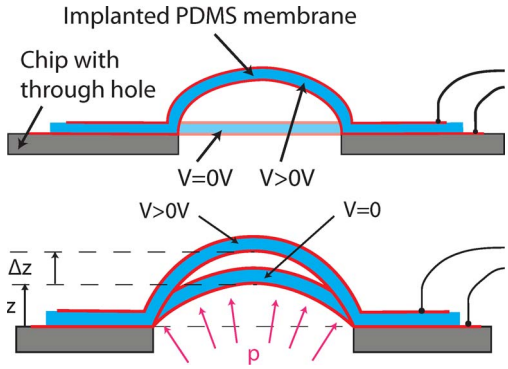

Fig. 3. (Top) Buckling-mode DEA actuator. When a voltage is applied to the initially flat actuator, the electrostatic stress causes the structure to buckle, due to the clamped boundary conditions at the membrane's border, which prevent the in-plane area expansion. (Bottom) Same actuator submitted to a pressure on one side of the membrane. The equilibrium position is modified by a voltage applied between the electrodes.

The electrostatic pressure p_{el} which is generated on the electrode by a voltage V is defined by [9]

$$p_{\mathrm{el}} = \epsilon_0 \epsilon_r \left(\frac{V}{t}\right)^2 \tag{1}$$

where ϵ_0 and ϵ_r are, respectively, the vacuum and relative permittivity and t is the thickness of the dielectric layer. We use PDMS layers of thickness 15–40 μm to make our actuators, and voltages up to 2.5 kV are applied between the electrodes. A simple theoretical model describing the vertical deflection of circular buckling-mode DEAs submitted to an electric field and a mechanical distributed load over the membrane (pressure) was introduced in [20]. The model was slightly modified to better describe our polymeric circular membrane's deformation when submitted to a pressure difference, as described in [18] and shown in the bottom of Fig. 3, which leads to

$$p = \frac{8(1-0.24\nu)Yt_0}{3(1-\nu)(r^2+z^2)^2}z^3 + \frac{4\sigma_0 t_0 r^2}{(r^2+z^2)^2}z - \frac{4\epsilon_0\epsilon_r V^2}{t_0 r^2}z \tag{2}$$

relating the applied pressure p, the out-of-plane deflection of the membrane's center z, and the applied voltage V. ν is the Poisson ratio, Y is the PDMS' Young's modulus, t_0 is the initial thickness of the membrane, r is its radius, and σ_0 is the membrane's residual stress. The case where $p = 0$ represents the special case of the buckling-mode actuator, i.e., in the absence of an external pressure. The case where $V = 0$ represents the deflection of the membrane due to a pressure difference, in the absence of an applied voltage. A graphical representation of (2), calculated for a membrane representative of our actuators, is shown on Fig. 4. The dotted line shown in the figure represents the behavior of an unloaded membrane (no external force), in which case the model predicts no displacement up to a buckling threshold voltage V_b, where elastic instability occurs and out-of-plane motion is observed.

B. Actuators Fabrication

The actuators were fabricated at the chip level, to limit implantation time with the scanned 1-cm^2 beam. The process flow is shown in Fig. 5 and consists of implanting and sputtering Au

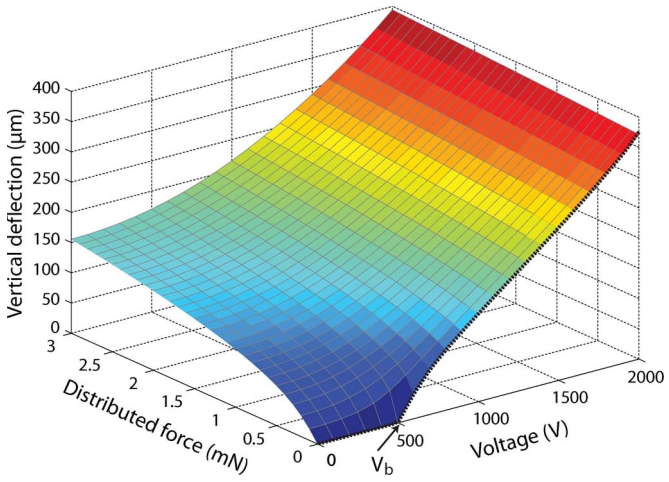

Fig. 4. Graphical representation of the theoretical vertical displacement of a ∅2-mm 20-μm-thick membrane with $Y = 2$ MPa, and $\sigma_0 = 20$ kPa.

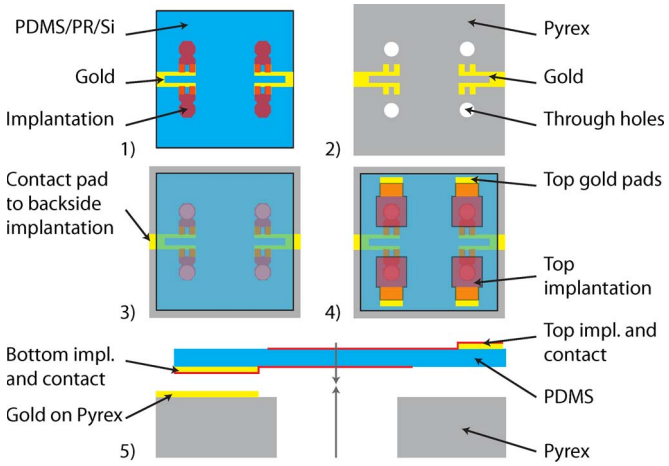

Fig. 5. Process flow for chip-scale fabrication of EPA membrane actuators. 1) PDMS is spun on Si wafer covered with PR, which is then diced into 18×18 mm^2 chips. Gold contacts are sputtered on the PDMS, followed by a first patterned implantation of what will be the backside of the membrane once assembled. 2) Holes are patterned with an UV laser through a Pyrex wafer, which is then diced into 20×20 mm^2 chips. Gold contacts are sputtered on the Pyrex chip. The gold contacts on the PDMS and on the Pyrex chip have the same shape. 3) The Si/PR/PDMS sandwich is bonded on the Pyrex chip. The two gold electrodes are aligned and put in contact during the bonding. The Si chip is removed by dissolution of the PR layer in acetone. 4) Topside gold contacts and implantation are added.

electrodes on both sides of a PDMS membrane, bonding it to a Pyrex chip on which corresponding Au contacts have been deposited. First, a 2-μm-thick PR layer is spun on a 4-in Si wafer to serve as sacrificial layer and baked on a hotplate for 1 min at 100 °C. Sylgard 186 from Dow Corning is prepared by mixing the PDMS with the curing agent with a 10 : 1 weight ratio, according to the manufacturer's indications. The mixture is then diluted with isooctane (PDMS : Solvent 10 : 9 weight) in order to lower its viscosity and spin-coated on the PR-coated Si wafer to obtain a PDMS thickness in the 20–30-μm range. The PDMS is left to cure at room temperature (in order to minimize the residual tensile stress in the layers) for two days. The wafer is then diced into 18×18 mm^2 chips. Gold electrodes that extend to the chip's edges are then sputtered on a PDMS chip and will serve as conduction path between the backside implanted zone

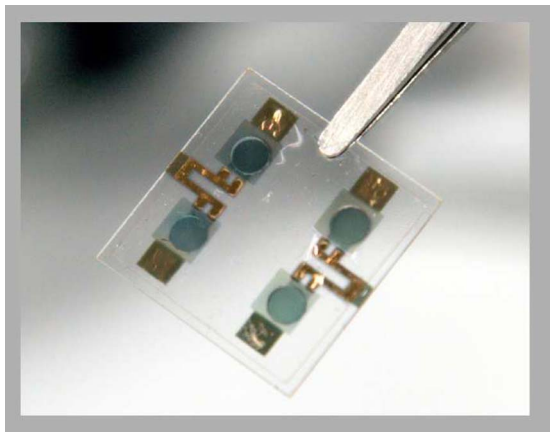

Fig. 6. Photograph of the finished chip with four actuators with ∅3-mm membranes.

and the chip's border. This is followed by a patterned implantation with Au ions through a steel shadow mask. Holes (∅1.5–3 mm) are drilled by UV laser machining into a Pyrex wafer, which is then diced into 20×20 mm^2, i.e., slightly larger than the PDMS chips. A gold-sputtered electrode, identical to the one made on the PDMS chip, is patterned on the Pyrex chip. The implanted PDMS is bonded on the Pyrex after an oxygen plasma treatment of both chips (15 s at 400 W and 2.45 GHz, with an O_2 flow of 400 sccm and at a pressure of ~500 mtorr). The implanted zones on the PDMS consequently form the backside electrode of the actuator. The silicon chip which lies above the PDMS layer is removed by dissolution of the sacrificial layer in acetone, thus creating freestanding membranes on the Pyrex chip. The process continues with the Au sputtering of contact electrodes on the PDMS topside, and the final step consists in a patterned topside implantation through a shadow mask. Wires are then added to the gold contact pads to bring charges on the two implanted electrodes. Each chip consists of four membranes which are independently addressable (Fig. 6).

Compared to the previous methods we used to make diaphragm DEAs [19], [20], the new process flow introduced in this paper presents several advantages. First, replacing the conductive silicon chip by an insulating Pyrex chip allows us to apply roughly twice the voltage to the membrane before dielectric breakdown occurs. As shown schematically in Fig. 7, the PDMS is mechanically deformed (thinned) when a metal contact wire is bonded to a gold contact pad on the PDMS. This local thinning reduces the breakdown voltage across the PDMS in the region between contact pad and grounded silicon chip. The increase in applied voltage brought by the new design enabled us to increase the displacement of our actuators by a factor of four.

Additionally, the new process flow introduces a patterned backside electrode which is connected to the power supply by a low-resistance gold strip. Much lower RC time constants are consequently obtained with this design, compared to relying on the poor electrical contact between the backside implantation and the Si chip as was done in our previous process flow. The slow response time obtained with our previous actuators (15–500 ms) combined with an actuator capacitance around 10 pF indicates that the series resistance of the actuator was in the

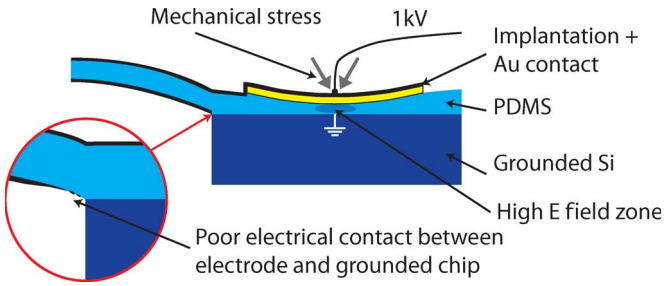

Fig. 7. Illustration of the problems present in our previous process flow based on Si chips [19], [20] and that are solved using the process flow shown in Fig. 5. 1) The mechanical deformation of the PDMS induced by the topside electrical contacts over a grounded conductive substrate (Si) led to a higher electric field under the contact pad than in the *active* part of the actuator, leading to dielectric breakdown between the contact pad and the silicon chip at voltages well below the breakdown voltage of the active area. 2) The through-hole backside implantation lead to a poor electrical contact between the implanted electrode and the hole's walls, thus leading to a high RC constant of the actuator. The series resistance of the RC circuit was estimated to $10^{10}\ \Omega$.

range of $10^{10}\ \Omega$ and that the contact between the bottom implantation and the chip was of very bad quality (Fig. 7). The response speed, which was electrically limited on our previous devices because of this issue, is now mechanically limited, as exposed later in Section IV.

Because our actuator's electrodes have roughly the same size as the freestanding membranes, steel shadow masks were used for the patterning of the implanted zone. This technique has many advantages, including cost, processing time, simplicity, and reusable masks. However, shadow masks also impose some limitations, such as the inability to make complex shapes such as rings as well as a limited resolution ($\approx$100 μm). For such cases, photolithography can be used to pattern a PR mask on the PDMS. Implantation is then conducted on/through the developed PR mask, which is then removed with acetone. Fig. 8 shows the possibility to pattern the implantation by photolithography. Our laboratory logo, which involves lines as small as 43 μm, coupled with annular shapes, has been patterned by photolithography and implanted. The figure also shows the possibility to deform the implanted PDMS.

Photolithography on PDMS layers is not as straightforward as when conducted on hard substrates, such as silicon. Standard photolithography process flows used by the microelectronics and MEMS community usually include baking steps in an oven or on a hotplate before the UV exposure and after the development. However, after spin-coating a thin (1–2 μm) PR layer on PDMS, exposition to heat should be avoided. Indeed, PDMS's high coefficient of thermal expansion ($\sim 10^{-3}\ \mathrm{K}^{-1}$) induces a large dilatation which leads to cracking and damage to the PR layer. To solve this problem, the PR's solvents were not removed by heating the substrate but by placing it in a vacuum chamber for 12 h. After the pattern's development, no postbake was conducted, again to avoid thermally induced stress and defects in the PR layer.

IV. Results

A. Static Displacement

Static out-of-plane deflection of the diaphragm actuators was characterized (Fig. 9). The vertical motion as a function of the

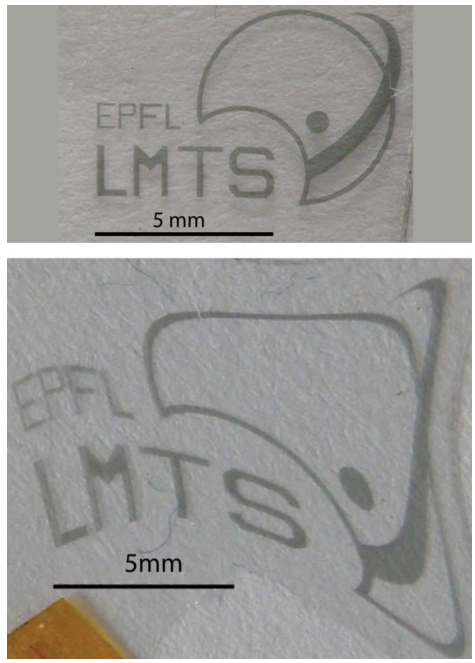

Fig. 8. (Top) Undeformed Au implantation of the laboratory's logo, patterned by photolithography. The smallest dimension (43 μm) and the annular shapes make it impossible to obtain this layout with a steel shadow mask. (Bottom) Same as top but stretched after implantation.

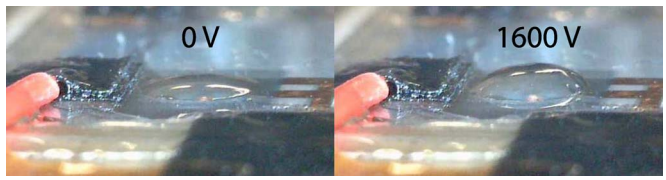

Fig. 9. ∅3-mm membrane actuator at (left) 0 V and (right) 1600 V. A pressure of 125 Pa was applied under the membrane to promote upward displacement, which is why the membrane is not flat at 0 V. The contacting wire to the upper electrode is visible on the left side of the photograph.

applied voltage and in the absence of a mechanical biasing force was measured with a white-light optical profiler Wyko NT1100 from Veeco. The characteristics obtained for three Pyrex actuators of different diameters are shown in Fig. 10. For comparison, the deflection of an actuator on Si obtained by the process flow described in [20] is also represented. As it can be observed on the graph, the much higher voltage that can be applied to the Pyrex actuators enables to obtain displacements that are four times larger than our previous reported results, reaching up to 25% of the membrane's diameter. The mechanical and geometrical parameters of the four actuators were measured with a bulge test setup and are summarized in Table I. The higher displacement of the Si actuator at identical voltage, compared to its same-size Pyrex conterpart, is due to the use of a softer PDMS (Nusil CF19-2186) for the actuator on Si as well as a smaller membrane thickness. This suggests that even greater unloaded displacements could be obtained by the use of a softer polymer with the present process flow.

The buckling threshold predicted by the theoretical model in the case of unloaded displacement [(2) and Fig. 4] is rarely clearly observed on these elastomeric actuators. Out of the four devices shown in Fig. 10, only the ∅3-mm Pyrex actuator

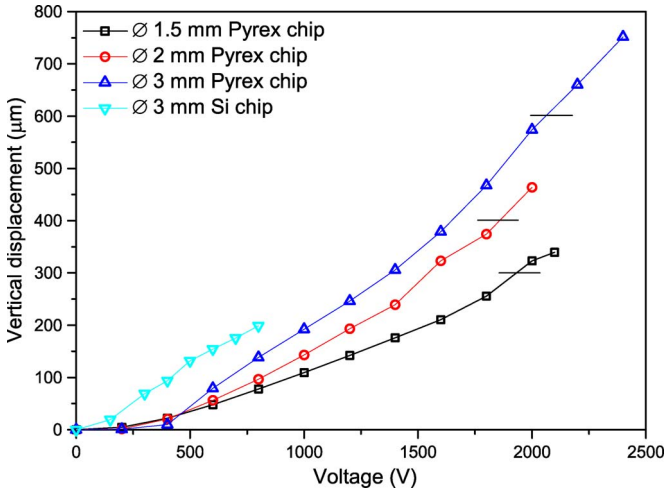

Fig. 10. Out-of-plane deflection of the membrane's center for different actuator diameters and chip materials. The Si-chip actuator, reported in [20], fails at much lower electric field and exhibits a maximum displacement four times lower than an actuator of similar size on Pyrex. The horizontal black lines indicate a displacement-over-diameter ratio of 20%.

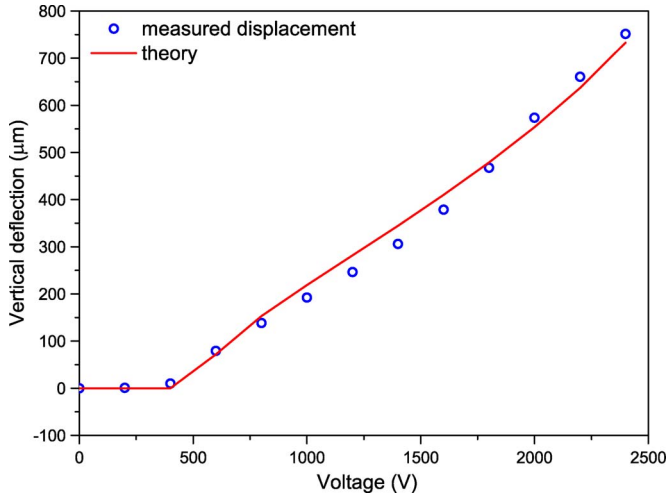

Fig. 11. Vertical deflection versus voltage for the ∅3-mm Pyrex actuator, and theoretical model (2). The geometric and mechanical parameters of the membrane are as follows (Table I): $Y = 2.4$ MPa, $\sigma_0 = 11$ kPa, and $t_0 = 26$ μm. A Poisson ratio of 0.5 (incompressible materials) was used.

TABLE I
MECHANICAL PARAMETERS OF THE FOUR MEMBRANES USED FOR THE UNLOADED OUT-OF-PLANE DEFLECTION MEASUREMENT SHOWN IN FIG. 10

Actuator	t_0 (μm)	Y (MPa)	σ_0 (kPa)
∅1.5 mm Pyrex	25.0	2.6	11
∅2 mm Pyrex	17.5	2.4	22
∅3 mm Pyrex	26.0	2.4	11
∅3 mm Si	22.5	0.8	17

clearly shows no displacement up to 400 V, whereas the three other exhibit an out-of-plane deflection even at low voltages. This is due to the initial few micrometer of waviness of the membranes, which promotes displacement before the buckling threshold is reached. The theoretical model (2), with $p = 0$, was applied to the measured data points of the ∅3-mm device and is in excellent agreement with the observed values (Fig. 11). The effectiveness of the model is important as it then allows membrane parameters to be chosen and optimized for different applications, for instance, accepting reduced displacement in exchange for larger force or immediately visualizing the predicted performance of different elastomers.

The deformation profile along the membrane's diameter is shown in Fig. 12 for a ∅2-mm actuator. It is shown that, in that case, the initial membrane's deformation promotes downward motion. Measurements of the membrane's deflection profile for voltages higher than 1200 V was not possible, due to a slope near the membrane's border exceeding the capabilities of our white-light optical profiler. The motion direction can be imposed by applying a small pressure on one side of the membrane, as shown in Fig. 9. However, the measurement shown in Figs. 10–13 was obtained without any biasing force.

The out-of-plane deflections of four ∅2-mm membranes cofabricated on the same chip are shown in Fig. 13. The very similar displacement versus voltage characteristics for the four membranes shows that we obtain a good uniformity of the actuators' properties on the whole chip surface. This concerns both

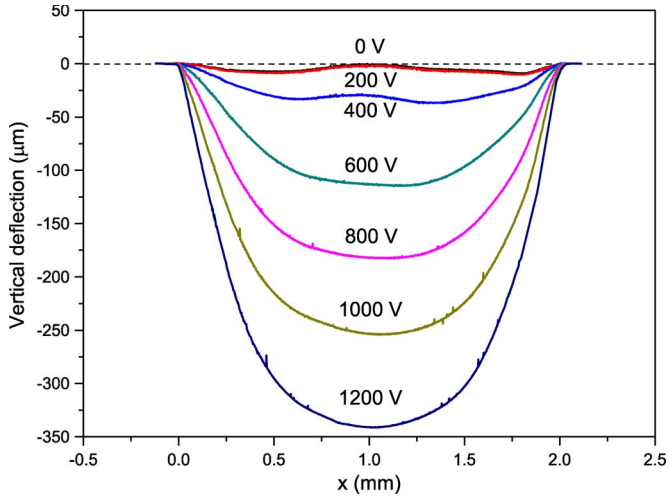

Fig. 12. Cross section of a ∅2-mm downward-moving membrane for different voltage values. The cross section shows the initial micrometer-scale waviness of the membrane, which promotes downward motion.

the PDMS thickness homogeneity and the stiffening impact of implantation. These results show that the scanning stage used during the implantation is effective in obtaining a uniform ion dose across all the membranes. The saturation of the deflection versus voltage curve, visible on the figure for voltages above 1500 V and not predicted by the theory, is attributed to the influence of the interaction between the membrane and the hole's walls. It is indeed observed uniquely on downward-deflecting membranes.

The stability of the actuator's static deflection was investigated by recording the buckling height of a ∅3-mm actuator over a 24-h period.At time $t = 0$, the voltage is switched from 0 to 1500 V, resulting in a rapid jump from the membrane to a height of 330 μm, which is then followed by a slower increase up to a height of 380 μm ($+50$ μm) over a 30-min period. This further increase of the deflection at a slow rate is attributed to stress-induced alignment of the polymer chains. After this stabilization period, the height of the membrane remains very stable over the 20+ h of the test. When the voltage is removed,

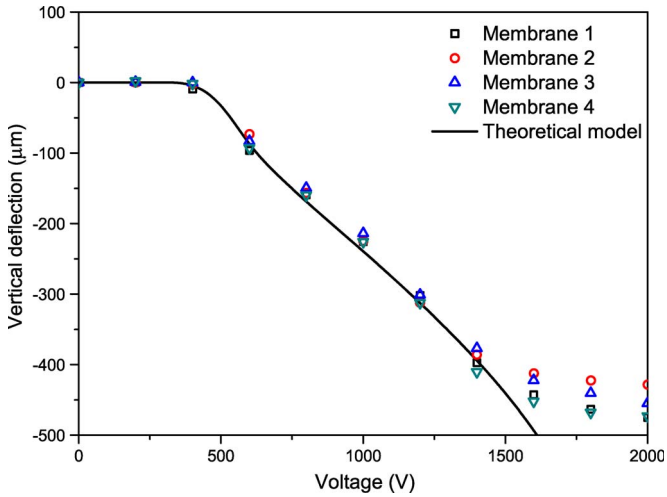

Fig. 13. Out-of-plane deflection of four ∅2 mm located on the same chip as well as the theoretical model for $Y = 2.4$ MPa, $\sigma_0 = 22$ kPa, and $t_0 = 17$ μm. The fact that the four chips exhibit very similar displacement versus voltage characteristics shows that the PDMS properties, as well as the impact of implantation, are homogeneous over the whole chip. The saturation at −500 mm for these downward-buckling devices is explained in the text.

the membrane quickly goes back to a height of 50 μm, and it takes again approximately 30 min until the membrane returns to its original flat position.

Degradation of the deflection after a large number of cycles was also investigated: two ∅3-mm actuators were submitted to a 1500-V step signal, and the resulting out-of-plane displacement's amplitude was recorded. The actuators were then activated at 20 Hz up to a height of 50 μm for a large $(> 10^6)$ number of cycles. The deflection's height resulting from a 1500-V voltage step was again measured at the end of the test. The results show that the static deflection's amplitude reached after a large number of cycles is not decreased but even exhibits a slight increase, which is attributed to chains rearrangements in the polymer (Table II).

B. Dynamic Response

We had observed response times ranging between 15 and 500 ms for our actuators on silicon chips [20]. This slow response, and large variation between the actuators, is attributed to the unreliable electrical contact between the backside implanted electrode and the Si chip, thus causing a large RC time constant, varying from chip to chip. The process flow for the Pyrex-based devices reported in this paper was designed to ensure a low-resistance contact and, hence, an RC time much shorter than the mechanical response time. Dynamic characterization of the new chips on Pyrex was performed by measuring the transient response to an HV step with a laser Doppler vibrometer (*Polytec MSV-400*). A dc HV supply whose output was controlled by an HV MOSFET was used to generate the input step signal.

The frequency response was also measured with the laser Doppler vibrometer by applying a sinusoidal excitation signal with a dc component, in order to obtain a motion at the same frequency than the electrical input signal. All the dynamic measurements were conducted without any applied mechanical force on the membranes.

Fig. 14 shows the displacement of the membrane's center for a ∅2-mm actuator. The electrical excitation was a 700-V square signal at 1 Hz. The good electrical contact to the backside electrode allows a high current flow into the circuit, rapidly bringing the charges on the electrodes, thus leading to short electrical time constant and a mechanically dominated behavior. As silicon presents a lower viscoelasticity compared to acrylic elastomers also commonly used to make DEAs [27], [28], much shorter response times can be obtained. A closer look at the voltage transition zone (Fig. 15) shows a mechanically underdamped behavior with oscillations at 1350 Hz, which corresponds to the mechanical resonance frequency of the actuator. The frequency response of the actuator when excited with a sinusoidal signal (Fig. 15, inset) shows a completely flat response, up to the mechanical resonance frequency of the actuator. We therefore have two time constants: one short one (in milliseconds) corresponding the motion of the membrane ignoring viscoelasticity and polymer rearrangement and a much longer one (15 min) that we attribute to relaxation processes in the silicon elastomer. The short time constant corresponds to roughly 85% of the displacement, the longer time constant to the remaining 15%.

V. Conclusion

We have used low-energy metal ion implantation to fabricate millimeter-size DEAs on Pyrex chips, capable of out-of-plane deflection up to 25% of their diameter and with response time on the order of milliseconds. We have presented a new process flow for the actuators' fabrication, which leads to vertical displacements 4.5 times higher as compared to our previous reported results as well as a much shorter response time. With unpatterned thin-film electrodes on devices of similar size, Pimpin *et al.* [16] obtained vertical-displacement-over-diameter ratio of 0.5%, which was increased to 5.6% with optimized thin-film electrodes patterned in concentric rings. The 25% vertical-displacement-versus-diameter ratio that we obtain with compliant metal ion-implanted electrodes illustrates the reduced membrane stiffening impact of this technique, compared to conventional thin-film deposition. Carpi *et al.* [29] have experimented with macroscale (∅3 cm) nonprestretched silicon buckling-mode actuators with carbon-based electrodes. They use a much softer silicon rubber than ours $(Y = 50$ kPa), but the maximal applied electric field at breakdown is also considerably reduced. With their devices, they obtained vertical displacement up to 22.7% of the actuator's diameter, which is very similar to the results presented in this paper, thus showing that miniaturization and the implantation-induced stiffening does not hinder the actuator's performances. The theoretical maximal out-of-plane deflection achievable on these buckling-mode actuators based on nonprestreched elastomers is limited by the pull-in phenomenon, which leads to dielectric breakdown. With a simple purely elastic material model, this phenomenon occurs for a thickness strain of −33%, which corresponds to a vertical-deflection-over-diameter ratio of 35%. Further optimization of our actuators can probably lead to displacements approaching this theoretical limit.

TABLE II
STATIC DEFLECTION MEASURED ON TWO ∅3 mm BEFORE AND AFTER A LARGE NUMBER OF CYCLIC ACTUATION AT 20 Hz

Sample	initial deflection (μm)	number of cycles	final deflection (μm)
1	231	1872000	247
2	359	1296000	371

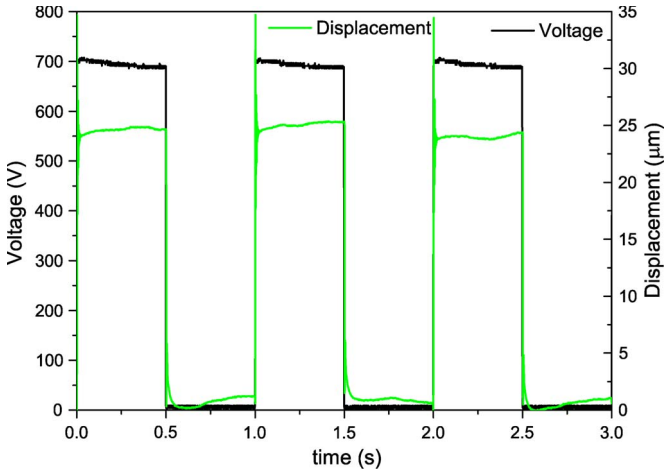

Fig. 14. Dynamic response to a 1-Hz 700-V step signal for a ∅2-mm actuator on a Pyrex chip. Measurement of the displacement of the membrane's center. The membranes' overshoots and rings.

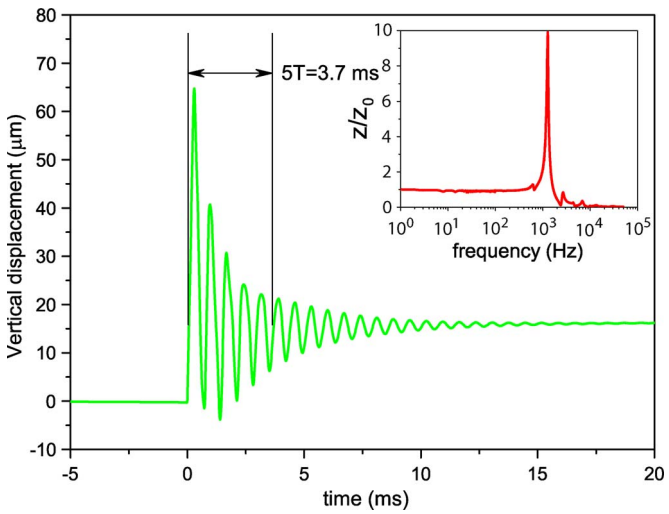

Fig. 15. Measured displacement during one 0–700-V voltage step (zoom on a part of Fig. 14). A mechanically underdamped behavior is observed. The oscillations have a frequency of 1350 Hz. (Inset) Frequency response of the actuator measured by applying a 250-V zero-to-peak ac signal to the device. One observes a flat response up to the mechanical resonance frequency of the membrane, characteristic of a second-order system.

Patterned compliant electrodes are necessary for the fabrication of miniaturized DEAs. The mainstream techniques to make electrodes for DEAs can only be used with great difficulty to create electrodes patterned on the millimeter scale or smaller, and consequently, research on miniaturized DEAs has been lagging. Ion implantation, coupled with the use of a shadow mask or a photolithographically defined PR mask, was shown in this paper to be an efficient method to create compliant and patternable electrodes which opens the way to DEAs' miniaturization.

One of the downsides of DEAs is the HV that needs to be applied for actuation. For safety reasons, HVs are a concern for the use of DEAs in consumer goods. It is possible to decrease the voltage by using a softer polymer (lower Young's modulus) or by using thinner membranes. However, these two approaches weaken the actuator, whose output force capabilities will decrease. A multilayer structure with alternating dielectric and electrode layers [14], [30] allows the keeping of the overall actuator's stiffness unchanged while decreasing the actuation voltage. Because ion implantation leads to very thin electrodes (around 50 nm, inside the dielectric) that can easily be patterned, they could advantageously be used to make stacked DEAs.

Our suspended membranes' fabrication process is based on the bonding of an elastomer layer on a chip patterned with through holes instead of the more conventional scheme commonly used to fabricate thin-film suspended membranes, which consists in depositing the membrane's material on a substrate, with a subsequent back etching of the substrate to free the membranes. This standard process has been successfully applied to the fabrication of thin suspended PDMS membranes [16], [31], but our bonding process advantageously gives us access to the backside of the implanted membrane just before the bonding step. This allows us to implant the backside electrode before bonding the membrane on the chip, thus ensuring a good electrical contact to this electrode and, hence, RC time constants shorter than mechanical time constants. The large displacement actuator reported in this paper, coupled with the currently demonstrated ability to pattern the implantation with a PR-based process in addition to a shadow mask technique, will allow the development of large arrays of submillimeter-size EAP actuators on chips for applications such as arrays of individually tunable microlens, micropump arrays for self-contained lab-on-chip, and arrays of single-cell manipulators.

ACKNOWLEDGMENT

The authors would like to thank Dr. Dadras, CSEM, for access to the gold-sputtering equipment.

REFERENCES

[1] S. Ashley, "Artificial muscles," *Sci. Amer.*, vol. 289, no. 4, pp. 52–59, 2003.
[2] F. Carpi, D. D. Rossi, R. Kornbluh, R. Pelrine, and P. Sommer-Larsen, Eds., *Dielectric Elastomers as Electromechanical Transducers*. Amsterdam, The Netherlands: Elsevier, 2008.
[3] G. Kovacs, P. Lochmatter, and M. Wissler, "An arm wrestling robot driven by dielectric elastomer actuators," *Smart Mater. Struct.*, vol. 16, no. 2, pp. S306–S317, Mar. 2007.
[4] F. Carpi, A. Mannini, and D. D. Rossi, "Elastomeric contractile actuators for hand rehabilitation splints," in *Proc. SPIE EAPAD*, Y. Bar-Cohen, Ed., 2008, vol. 6927, p. 692705.
[5] V. Sujan and S. Dubowsky, "Design of a lightweight hyper-redundant deployable binary manipulator," *J. Mech. Des.*, vol. 126, no. 1, pp. 29–39, Jan. 2004.

[6] A. Wingert, M. Lichter, S. Dubowsky, and M. Hafez, "Hyper-redundant robot manipulators actuated by optimized binary-dielectric polymers," in *Proc. SPIE Int. Soc. Opt. Eng.*, 2002, vol. 4695, pp. 415–423.
[7] J. Vogan, A. Wingert, J. S. Plante, S. Dubowsky, M. Hafez, D. Kacher, and F. Jolesz, "Manipulation in MRI devices using electrostrictive polymer actuators: with an application to reconfigurable imaging coils," in *Proc. IEEE ICRA*, 2004, vol. 3, pp. 2498–2504.
[8] S. Michel, A. Bormann, C. Jordi, and E. Fink, "Feasibility studies for a bionic propulsion system of a blimp based on dielectric elastomers," in *Proc. SPIE EAPAD*, Y. Bar-Cohen, Ed., 2008, vol. 6927, p. 69270S.
[9] R. E. Pelrine, R. D. Kornbluh, and J. P. Joseph, "Electrostriction of polymer dielectrics with compliant electrodes as a means of actuation," *Sens. Actuators A, Phys.*, vol. 64, no. 1, pp. 77–85, Jan. 1998.
[10] F. Carpi, P. Chiarelli, A. Mazzoldi, and D. De Rossi, "Electromechanical characterisation of dielectric elastomer planar actuators: Comparative evaluation of different electrode materials and different counterloads," *Sens. Actuators A, Phys.*, vol. 107, no. 1, pp. 85–95, Oct. 2003.
[11] B. O'Brien, J. Thode, I. Anderson, E. Calius, E. Haemmerle, and S. Xie, "Integrated extension sensor based on resistance and voltage measurement for a dielectric elastomer," in *Proc. SPIE EAPAD*, San Diego, CA, 2007, vol. 6524, pp. 652415-1–652415-11.
[12] M. Aschwanden and A. Stemmer, "Low voltage, highly tunable diffraction grating based on dielectric elastomer actuators," in *Proc. SPIE EAPAD*, San Diego, CA, 2007, vol. 6524, pp. 65241N-1–65241N-10.
[13] H. Schlaak, M. Jungmann, M. Matysek, and P. Lotz, "Novel multilayer electrostatic solid-state actuators with elastic dielectric," in *Proc. SPIE EAPAD*, 2005, vol. 5759, pp. 121–133.
[14] M. Matysek, P. Lotz, T. Winterstein, and H. Schlaak, "Dielectric elastomer actuators for tactile displays," in *Proc. World Haptics 3rd Joint EuroHaptics Conf. Symp. Haptic Interfaces Virtual Environ. Teleoperator Syst.*, 2009, pp. 290–295.
[15] R. Pelrine, R. Kornbluh, J. Joseph, R. Heydt, Q. Pei, and S. Chiba, "High-field deformation of elastomeric dielectrics for actuators," *Mater. Sci. Eng. C*, vol. 11, no. 2, pp. 89–100, Nov. 2000.
[16] A. Pimpin, Y. Suzuki, and N. Kasagi, "Microelectrostrictive actuator with large out-of-plane deformation for flow-control application," *J. Microelectromech. Syst.*, vol. 16, no. 3, pp. 753–764, Jun. 2007.
[17] M. Niklaus, S. Rosset, M. Dadras, P. Dubois, and H. Shea, "Microstructure of 5 keV gold-implanted polydimethylsiloxane," *Scripta Materialia*, vol. 59, no. 8, pp. 893–896, 2008.
[18] S. Rosset, M. Niklaus, P. Dubois, and H. Shea, "Metal ion implantation for the fabrication of stretchable electrodes on elastomers," *Adv. Funct. Mater.*, vol. 19, no. 3, pp. 470–478, 2009.
[19] P. Dubois, S. Rosset, S. Koster, J. Stauffer, S. Mikhailov, M. Dadras, N.-F. de Rooij, and H. Shea, "Microactuators based on ion implanted dielectric electroactive polymer (EAP) membranes," *Sens. Actuators A, Phys.*, vol. 130/131, pp. 147–154, Aug. 2006.
[20] S. Rosset, M. Niklaus, P. Dubois, and H. R. Shea, "Mechanical characterization of a dielectric elastomer microactuator with ion-implanted electrodes," *Sens. Actuators A, Phys.*, vol. 144, no. 1, pp. 185–193, May 2008.
[21] I. Aksenov, V. A. Belous, V. G. Padalka, and V. M. Khoroshikh, "Transport of plasma streams in a curvilinear plasma-optics system," *Sov. J. Plasma Phys.*, vol. 4, no. 4, pp. 425–428, Jul./Aug. 1978.
[22] S. Anders, A. Anders, and I. Brown, "Macroparticle-free thin films produced by an efficient vacuum arc deposition technique," *J. Appl. Phys.*, vol. 74, no. 6, pp. 4239–4241, Sep. 1993.
[23] S. Anders, A. Anders, and I. Brown, "Focused injection of vacuum arc plasmas into curved magnetic filters," *J. Appl. Phys.*, vol. 75, no. 10, pp. 4895–4899, May 1994.
[24] A. Anders, S. Anders, and I. G. Brown, "Effect of duct bias on transport of vacuum arc plasmas through curved magnetic filters," *J. Appl. Phys.*, vol. 75, no. 10, pp. 4900–4905, May 1994.
[25] I.G. Brown, "Vacuum arc metal plasma production and the transition of processing mode from metal ion beam to dc metal plasma immersion," *Surf. Coat. Technol.*, vol. 136, no. 1–3, pp. 16–22, Feb. 2001.
[26] A. Anders, S. Anders, and I. G. Brown, "Transport of vacuum arc plasmas through magnetic macroparticle filters," *Plasma Sources Sci. Technol.*, vol. 4, no. 1, pp. 1–12, Feb. 1995.
[27] P. Lochmatter and G. Kovacs, "Design and characterization of an active hinge segment based on soft dielectric EAPs," *Sens. Actuators A, Phys.*, vol. 141, no. 2, pp. 577–587, Feb. 2008.
[28] M. Aschwanden, D. Niederer, and A. Stemmer, "Tunable transmission gratings based on dielectric elastomer actuators," in *Proc. SPIE EAPAD*, San Diego, CA, 2008, vol. 6927, pp. 6927–6956.
[29] F. Carpi, G. Fantoni, P. Guerrini, and D. D. Rossi, "Buckling dielectric elastomer actuators and their use as motors for the eyeballs of an android face," in *Proc. SPIE EAPAD*, Y. Bar-Cohen, Ed., 2006, vol. 6168, p. 61681A.
[30] G. Kovacs and L. During, "Contractive tension force stack actuator based on soft dielectric EAP," in *Proc. SPIE EAPAD*, Y. Bar-Cohen and T. Wallmersperger, Eds., 2009, vol. 7287, p. 72870A.
[31] S. Sawano, K. Naka, A. Werber, H. Zappe, and S. Konishi, "Sealing method of PDMS as elastic material for MEMS," in *Proc. IEEE 21st Int. Conf. MEMS*, Jan. 13–17, 2008, pp. 419–422.

Samuel Rosset received the M.Sc. degree in microengineering and the Ph.D. degree from the Ecole Polytechnique Fédérale de Lausanne (EPFL), Lausanne, Switzerland, in 2004 and 2009, respectively.

In January 2009, he joined Optotune AG, a Swiss company which develops elastomeric adaptive optical elements. His domains of interest are in electroactive-polymer (EAP) actuators, compliant electrodes, and development of EAP- and elastomer-based products.

Muhamed Niklaus received the M.S. degree in physics from the Ecole Polytechnique Fédérale de Lausanne, Lausanne, Switzerland, in 2005, where he developed a theoretical model to describe configurations and scaling properties of DNA, and since 2006, has been working toward the Ph.D. degree in the field of nanocomplex produced by metallic ion implantation into polymers in the group of Prof. H. R. Shea in the Microsystems for Space Technologies Laboratory.

He develops an understanding of nanocomposites based on observations with high-magnification microscopes such as scanning probe microscopes, scanning electron microscopes, transmission electron microscopes, etc. He is the coauthor of two international publications on the subject of ion-implanted electroactive polymers.

Philippe Dubois received the Diploma degree in electricity/electronics from the University of Applied Sciences, Le Locle, Switzerland, and the Diploma degree in physics/electronics and the Ph.D. degree in microsystems from the University of Neuchâtel, Neuchâtel, Switzerland.

After two years of postdoctoral research on multidirectional accelerometers with the group of Prof. de Rooij, he joined the group of Prof. H. R. Shea in the Microsystems for Space Technologies Laboratory, Ecole Polytechnique Fédérale de Lausanne, Lausanne, Switzerland, where he has been leading research on dielectric electroactive elastomer actuators. Recently, he was an Independent Consultant for a research center. His domains of interest include silicon- and polymer-based microelectromechanical systems, artificial muscles, ion implantation, nanocomposites, wireless sensor networks, and space exploration.

Herbert R. Shea (M'00–SM'09) received the B.Sc. degree in physics from McGill University, Montreal, QC, Canada, and the M.A. degree in physics and the Ph.D. degree (1997) from Harvard University, Cambridge, MA.

After two years as a Postdoctoral Fellow at the IBM T. J. Watson Research Center, Yorktown Heights, NY, he joined Bell Laboratories, Lucent Technologies, Murray Hill, NJ, where he became the Technical Manager of the Microsystems Technology Group, specializing in microelectromechanical-systems (MEMS) reliability. Since April 2004, he has been an Assistant Professor at the Ecole Polytechnique Fédérale de Lausanne, Lausanne, Switzerland, where he founded the Microsystems for Space Technologies Laboratory. His current research topics include micromachined polymer MEMS actuators, electric micropropulsion, MEMS sensors for satellite attitude determination, chip-scale plasma sources, and picosatellites.